



Published in final edited form as:

Neuromodulation. 2023 June ; 26(4): 745–754. doi:10.1016/j.neurom.2022.10.045.

Targeted Modulation of Human Brain Interregional Effective Connectivity With Spike-timing Dependent Plasticity

Julio C. Hernandez-Pavon, PhD, DSc^{1,2,3}, Nils Schneider-Garces, MS², John Patrick Begnoche, MS², Lee E. Miller, PhD^{1,4,5,6}, Tommi Raij, MD, PhD^{1,2,7}

¹Department of Physical Medicine and Rehabilitation, Feinberg School of Medicine, Northwestern University, Chicago, IL, USA

²Center for Brain Stimulation, Shirley Ryan AbilityLab, Chicago, IL, USA

³Legs + Walking Lab, Shirley Ryan AbilityLab, Chicago, IL, USA

⁴Department of Physiology, Feinberg School of Medicine, Northwestern University, Chicago, IL, USA

⁵Department of Biomedical Engineering, McCormick School of Engineering, Northwestern University, Evanston, IL, USA

⁶Limb Motor Control Lab, Shirley Ryan AbilityLab, Chicago, IL, USA

⁷Department of Neurobiology, Weinberg College of Arts and Sciences, Northwestern University, Evanston, IL, USA

Abstract

Objective: The ability to selectively up- or downregulate interregional brain connectivity would be useful for research and clinical purposes. Toward this aim, cortico-cortical paired associative stimulation (ccPAS) protocols have been developed in which two areas are repeatedly stimulated with a millisecond-level asynchrony. However, ccPAS results in humans using bifocal transcranial magnetic stimulation (TMS) have been variable, and the mechanisms remain unproven. In this study, our goal was to test whether ccPAS mechanism is spike-timing-dependent plasticity (STDP).

Address correspondence to: Tommi Raij, MD, PhD, Center for Brain Stimulation, Shirley Ryan AbilityLab, 355 E Erie St, Chicago, IL 60611, USA. raij@nmr.mgh.harvard.edu.

Current address for Raij: MGH/MIT Athinoula A. Martinos Center for Biomedical Imaging, 149 13th St, Charlestown, MA 02129, USA.

Authorship Statements

Tommi Raij and Lee E. Miller conceived the study. Tommi Raij, Julio C. Hernandez-Pavon, and Lee E. Miller designed the experiments. Julio C. Hernandez-Pavon, Nils Schneider-Garces, John Patrick Begnoche, and Tommi Raij recruited the subjects, recorded the data, and contributed to data processing. Julio C. Hernandez-Pavon and Tommi Raij analyzed the EEG data, computed the statistics, and drafted the manuscript with important intellectual input from the other authors. All authors contributed to editing and revising and approved the final manuscript.

Conflict of Interest: The authors reported no conflict of interest.

SUPPLEMENTARY DATA

To access the supplementary material accompanying this article, visit the online version of *Neuromodulation: Technology at the Neural Interface* at www.neuromodulationjournal.org and at <https://doi.org/10.1016/j.neurom.2022.10.045>.

For more information on author guidelines, an explanation of our peer review process, and conflict of interest informed consent policies, please see the journal's [Guide for Authors](#).

Materials and Methods: Eleven healthy participants received ccPAS to the left primary motor cortex (M1) → right M1 with three different asynchronies (5 milliseconds shorter, equal to, or 5 milliseconds longer than the 9-millisecond transcallosal conduction delay) in separate sessions. To observe the neurophysiological effects, single-pulse TMS was delivered to the left M1 before and after ccPAS while cortico-cortical evoked responses were extracted from the contralateral M1 using source-resolved electroencephalography.

Results: Consistent with STDP mechanisms, the effects on synaptic strengths flipped depending on the asynchrony. Further implicating STDP, control experiments suggested that the effects were unidirectional and selective to the targeted connection.

Conclusion: The results support the idea that ccPAS induces STDP and may selectively up- or downregulate effective connectivity between targeted regions in the human brain.

Keywords

Cortico-cortical paired associative stimulation; diffusion MRI tractography; effective connectivity; electroencephalography; spike-timing dependent plasticity

INTRODUCTION

The human brain depends on appropriate long-range connectivity between cortical regions for normal behavioral function. Synaptic weights that influence connectivity are constantly adjusted in an experience-driven fashion.¹ Many psychiatric conditions involve synaptic changes in interregional connectivity strengths.² Similarly, white matter lesions, from, for example, stroke, disrupt specific axonal connections, which results in different deficits depending on the lesion site.^{3–7} Therefore, the ability to increase or decrease strengths of specific connections in a controlled manner would carry strong research and therapeutic potential.

In animal models, invasive cortico-cortical paired associative stimulation (ccPAS) has been explored for modulating connectivity in a controlled manner.^{8–10} ccPAS protocols stimulate two cortical areas with millisecond-level asynchrony. ccPAS is believed to invoke spike-timing-dependent plasticity (STDP), which is a temporally asymmetric N-methyl-D-Aspartate (NMDA) receptor-mediated form of Hebbian plasticity, extensively examined in a broad variety of neural preparations, including in cultured systems,¹¹ acutely prepared brain slices,^{12,13} and in vivo animal models.^{8–10,14,15} STDP is induced by stimulating presynaptic and postsynaptic sides of the target synapse with slight temporal offsets; the millisecond-level order of pre- vs postsynaptic activations determines whether synaptic strength is increased or decreased.

In humans, ccPAS has been applied noninvasively by delivering bifocal transcranial magnetic stimulation (TMS) pulses.^{16–18} Results in healthy participants suggest that it may be possible to use ccPAS to modulate behaviors associated with specific connections,^{19,20} and even clinical applications may emerge.^{21,22} However, ccPAS mechanisms in humans remain unproven.^{23–25} Mechanistic knowledge is needed because the required stimulation asynchrony critically depends on whether the mechanism is STDP. Furthermore, spatiotemporally accurate neurophysiological outcome measures that could quantify ccPAS

synaptic effects—and therefore reveal the mechanisms—are lacking. A related problem is that axonal interregional conduction delays, which need to be considered, are poorly characterized in humans.

In this study, with the goal of examining these issues, we 1) study in humans whether ccPAS induces cortical synaptic changes in effective connectivity through STDP and 2) develop a spatiotemporally accurate, noninvasive neurophysiological outcome measure to capture the effects that could also 3) reveal the axonal conduction delays. Figure 1 schematically illustrates our experimental model that includes synaptic-level modulations that, when many synapses are affected, can be detected extracranially with electroencephalography (EEG). Figure 1 (left) shows bifocal TMS of areas A and B that are axonally connected through the corpus callosum, for example, the left and right hemisphere primary motor cortices (M1s).^{26–28} Figure 1 (right) depicts the effect of asynchrony values on a target synapse in area B. Area A is stimulated at $t = 0$ milliseconds, leading to secondary activation of the presynaptic terminals in area B after a conduction delay. The transcallosal axonal conduction delay from left M1 \rightarrow right M1 is known, on the basis of bifocal interhemispheric inhibition studies, to be approximately 9 milliseconds.^{29,30} In experimental condition 1 (top), a TMS pulse to B is delivered at $t = 14$ milliseconds, which causes the presynaptic axon terminals to activate 5 milliseconds before the postsynaptic elements. According to STDP rules,¹¹ this leads to long-term potentiation at the target synapse. In experimental condition 2 (middle), B is stimulated at $t = 9$ milliseconds, causing the pre- and postsynaptic elements to be activated at the same time, leading to no change in synaptic efficacy.¹¹ Experimental condition 3 (bottom) delivers a TMS pulse to B at $t = 4$ milliseconds, consistent with long-term depression in the STDP framework.¹¹

MATERIALS AND METHODS

Participants

The inclusion criteria were as follows: healthy, aged 18 to 85 years, right-handed,³¹ and normal (corrected) vision and hearing. The exclusion criteria were any contraindications to TMS or magnetic resonance imaging (MRI); neurological, psychiatric, or other relevant medical problems; and medications influencing brain function.³² All experimental procedures were approved by the Northwestern University Institutional Review Board and were in accord with the Declaration of Helsinki ([ClinicalTrials.gov](https://clinicaltrials.gov/ct2/show/study/NCT03723434) Identifier [NCT03723434](https://clinicaltrials.gov/ct2/show/study/NCT03723434)). Participants gave their written informed consent at enrollment. Fourteen participants took part in the ccPAS recordings. Of these, data from three were removed, two owing to EEG instrument technical reasons (in one, EEG was recorded with different settings, and in another, the reference electrode was broken) and one because the TMS-evoked responses were too strongly contaminated by muscle artifacts. This resulted in a final sample of 11 subjects for whom TMS–EEG data were available (seven women, mean age 33 ± 14 years).

Experimental Design

The model in Figure 1 results in three predictions if the mechanism is indeed STDP. First, the effects on synaptic efficacy, as measured with postsynaptic potentials (PSPs), should be

temporally specific because they flip from increased to decreased when the order of pre- vs postsynaptic activation in the target synapse is reversed.^{16,17,33} This hypothesis was tested in the main experiment. Second, the effects should be unidirectional ($A \rightarrow B$ but not $B \rightarrow A$) because the target synapses with pre- to postsynaptic delays that should induce STDP are in area B, not in area A. Third, in area C (not shown), there should be no STDP because it does not receive TMS, indicating spatial selectivity ($A \rightarrow B$ but not $A \rightarrow C$). These predictions were tested in control experiments.

Experimental Design: Main Experiment

Figure 2 shows the design of our main experiment. In 11 healthy volunteers, changes caused by ccPAS were observed by recording the strengths of the target synapses in right M1 before and after ccPAS. These were obtained by delivering single-pulse TMS (spTMS) to the left M1 while measuring cortico-cortical evoked potentials (ccEPs) from the right M1. To extract the ccEPs from right M1 in a spatially and temporally selective manner, source-space EEG was used.³⁴ EPs reflect PSPs—particularly those of pyramidal neuron apical dendrites—and therefore measure synaptic strengths.^{35,36} If ccEP amplitudes from right M1 increase after ccPAS, effective connectivity left M1 \rightarrow right M1 increases; conversely, if the ccEP response amplitudes from right M1 decrease before vs after ccPAS, effective connectivity left M1 \rightarrow right M1 decreases. The ccEP time courses were further examined to see whether they would agree with the a priori knowledge of having an onset at approximately 5 milliseconds and peaking at approximately 9 milliseconds.^{29,30}

Experimental Design: Control Experiments

To further clarify whether the mechanism was STDP, we conducted three control experiments. First, because the transcallosal connections between left and right M1 are reciprocal,³⁷ we tested whether STDP-related connectivity changes were unidirectional by delivering spTMS to the right M1 (in separate runs from those in which spTMS was delivered to the left M1) and extracting ccEPs from the left M1. Supplementary Data Figure S1 shows that in left M1, the pre- to postsynaptic delays are different from right M1 because they are always negative ($-23/-18/-13$ milliseconds for the asynchrony conditions 14/9/4 milliseconds, respectively) and mainly outside the rather narrow pre- vs postsynaptic timing window in which STDP is expected to occur.¹¹ Second, to test whether any STDP-type effects showed spatial specificity, we also extracted the ccEPs from a nearby control region in the prefrontal cortex (right hemisphere pars orbitalis, from the anatomical a priori parcellation in FreeSurfer) from the data in which spTMS had been delivered to the left M1. Third, we also recorded motor evoked potentials (MEPs) from the left hand when spTMS was delivered to the right M1.

Although the goal was to record each participant with all three asynchronies, not all subjects were available for all conditions, mainly because of the need for multiple lengthy visits for each subject. From the total of 11 participants, eleven received ccPAS with an asynchrony of 14 milliseconds, seven with 9 milliseconds, and eight with 4 milliseconds. The order of visits was single-blinded and counterbalanced across participants with a break of at least seven days between them for washout. To assess the effects of ccPAS, as well as the conduction delays, we recorded spTMS-evoked EEG responses before (Before) and at ~ 10

(After[1]) and ~60 (After[2]) minutes after ccPAS (Fig. 2). For the spTMS runs before and after the ccPAS run, we stimulated the left M1 (shown in Fig. 2) and right M1 (not shown in Fig. 2) in separate runs. In addition, MEPs were recorded from the contralateral hand (first dorsal interosseus [FDI]).

During TMS, the participants wore earplugs for hearing protection. We first found the resting motor threshold (rMT) for the left and right primary motor cortex (M1) for the contralateral FDI muscle. The rMT was determined as the lowest TMS intensity evoking MEPs with an amplitude $> 50 \mu\text{V}$ peak-to-peak in at least five of ten consecutive trials.³⁸ Within subjects, the rMTs were stable across visits (3.8% for the left hemisphere and 3.1% for the right hemisphere; SD divided by the mean).

Structural MRI Recordings: T1-Weighted Images and Diffusion MRI

For TMS navigation, EEG source analysis, and TMS electric field (E-field) computations, high-resolution 3D T1-weighted images of the head were obtained on a 3 T Siemens Prisma Scanner and a 64-channel receiver array (Siemens, Erlangen, Germany). The images were acquired using a Multi-Echo Magnetization-Prepared Rapid Acquisition Gradient Echo sequence ($T1/TR/TE1/TE2/TE3/TE4/\alpha = 1190/2400/1.87/3.75/5.63/7.51 \text{ ms}/7^\circ$, sagittal slice orientation, 0.8 mm or 1.0 mm isotropic resolution depending on the head size, 2xGRAPPA).³⁹ These data were available from all subjects. In addition, to observe the transcallosal axonal bundle connecting left and right M1 FDI representations with MRI tractography, subjects were scanned with whole-brain diffusion spectrum imaging⁴⁰ with simultaneous multislice sequence with 257 directions,⁴¹ 2 mm isotropic voxel size, and a grid scheme with 22 different nonzero b values ranging from 150 to 4000. These data were available from seven subjects; in the others, the MRI specific absorption rate limit was exceeded. The sequence contained, after three initial b_0 volumes, additional 12 interspersed b_0 volumes every 21 volumes (total of 271 volumes) that were used for motion correction during preprocessing (below).

MRI Analysis

The MRIs were processed with FreeSurfer (version 6.0)⁴² for segmentation, parcellation, and reconstruction of cortical surfaces. In addition, we used FreeSurfer and the minimum norm estimate (MNE) processing stream³⁴ to extract the inner skull, outer skull, and scalp surfaces for individually shaped boundary element models (BEMs) that were used for EEG source analysis and TMS E-field modeling (below). For probabilistic tractography, the individual level diffusion data were preprocessed with motion correction using the interspersed b_0 volumes, analyzed with FSL dtifit/bedpost,⁴³ and seeded with the individual level left and right M1 areas extracted from the TMS-induced E-fields (below). The seeded results were then normalized with the individual level seed volumes (a standard technique to remove bias from seed volume differences across subjects). Thereafter, group-level analysis used FreeSurfer nonlinear morphing techniques (`mri_cvs_register`) to spatially align the individual brains and tractography results to the CVS35 standard brain in Montreal Neurological Institute (MNI) space,^{44,45} followed by averaging of the results across subjects in this standard space.

Single-pulse TMS

spTMS was applied with a MagPro X100 with MagOption stimulator and a C-B60 figure-of-eight coil (MagVenture, Farum, Denmark). TMS was targeted with a neuronavigation system (Localite, St Augustin, Germany) using the individual MRIs. The participants received 80 biphasic pulses at 100% rMT to the left M1 while the EEG evoked responses were recorded during the Before, After[1], and After[2] conditions. Although using a stronger intensity (> 100% rMT) might have increased the ccEPs, increasing the intensity would also have strengthened the TMS-evoked artifacts,^{46–49} which would likely have hampered the ability to observe the responses starting already at 5 milliseconds after spTMS.

ccPAS Parameters and Tasks

ccPAS was applied with two MagPro X100 with MagOption stimulators and two small, highly focal figure-of-eight coils (Cool-B35, MagVenture). Each coil was attached to a high-performance two-stage liquid-based cooler (MagVenture). The first TMS pulse was delivered to the left M1 and the second pulse to the right M1, with an asynchrony of 14 milliseconds, 9 milliseconds, or 4 milliseconds in different sessions. A total of 180 biphasic ccPAS pulses were delivered at a rate of 0.2 Hz (15 minutes) at 120% rMT to the FDI cortical representations (Fig. 2). To control for attention and vigilance, the task was to count the ccPAS pulse pairs silently. The subjects were instructed to keep their eyes open, look straight ahead to a fixation cross, and blink as little as possible. At 120% rMT intensity and coil orientation perpendicular to the local curvature of the central sulcus, one should expect that the pyramidal neurons were mainly activated through the indirect (I) mechanism, although the direct (D) mechanism may somewhat contribute.⁵⁰ Regarding the conduction delay and optimal asynchrony, the mechanism should not influence the results because the latency difference between D- and I¹-waves is only approximately 1.3 milliseconds⁵⁰ whereas the asynchrony increments were clearly longer (5 milliseconds).

EEG Recordings

EEG was recorded with a TMS-compatible 64-channel system (NeurOne Tesla, Bittium, Kuopio, Finland). The EEG electrodes were placed according to the International 10–20 System⁵¹ in an elastic cap and referenced to the right mastoid. Electrooculogram was recorded with electrodes placed at the lateral canthus of each eye (horizontal) and above and below the right eye (vertical). Impedances of all electrodes were checked before each run and kept below 5 k Ω . The signals were acquired in DC mode, band-pass filtered from 0.16 Hz to 5 kHz, and digitized at a sampling rate of 20 kHz. All recordings were carried out inside a two-layer electrically shielded room (Gaven Industries Inc, Saxonburg, PA).

TMS–EEG Artifact Minimization

To minimize the electrical artifacts induced by spTMS, each EEG electrode lead was rotated to an orientation in which the induced currents from the TMS coil were minimal, that is, pointing away from the coil and perpendicular to the coil windings.⁵² Finally, the cap was covered with a layer of plastic wrap to reduce electrode/lead movement and prevent the electrode gel from drying out. To further control the artifacts, we also monitored the TMS-evoked EEG online to immediately detect and resolve any issues, used TMS-optimized

pellet electrodes (EasyCap GmbH, Herrsching, Germany) and an EEG instrument with a wide dynamic range, and performed minimal filtering.^{46,48}

Motor Evoked Potentials

For MEP recordings, 80 biphasic spTMS were administered to the right M1 at 100% rMT while MEPs were recorded from the left FDI (Bittium). The MEPs were averaged across trials, and peak-to-peak amplitudes were measured. These data were collected at the same time as the EEG data for the control experiment for directionality.

Coordinate System Alignment Between MRI, EEG, and TMS

After EEG preparation, the locations of each electrode, three fiducial landmarks (nasion and two preauricular points), and approximately 120 additional scalp surface points were recorded with the TMS navigation system (Localite, Bonn, Germany). The fiducial points were then identified from the structural MRIs for an initial coordinate system alignment. Using the scalp surface points, this initial approximation was refined using an iterative closest point search algorithm.³⁴

TMS-induced E-fields

TMS-induced E-fields at left and right M1 were computed using our published techniques that combine the coil winding geometry and navigator data with individually shaped BEMs (single-layer at the inner skull) extracted from each participant's MRIs.^{53,54} The E-fields were computed at the gray-white matter surface of the individual anatomy and thresholded at 80% of the maximum value.

EEG Preprocessing and Evoked Responses

EEG analysis was performed offline with MATLAB (The Mathworks, Inc, Natick, MA) and the MNE processing stream.³⁴ The data were detrended, and the traces were visually inspected. Next, bad channels (eg, containing high noise level, strong muscle/eye movement, or nonresponsive) and bad trials (amplitudes exceeding $\pm 30 \mu\text{V}$ or excessive muscle activity from eye blinks or scalp/neck muscles, in the time window -200 to $+100$ milliseconds) were removed. Thereafter, the evoked responses were averaged time locked to the spTMS pulses ($t = 0$ milliseconds) in a time window of -200 to $+300$ milliseconds. To make interpretation straightforward and avoid known confounds, we did not use signal processing algorithms for attempting to suppress artifacts in TMS-evoked EEG data.^{49,55-58}

EEG Source Analysis

Source analysis of the spTMS-evoked EEG responses was conducted with the MNE magneto/electroencephalography processing stream.³⁴ The individual level three-layer BEMs (with inner skull, outer skull, and scalp) extracted from the MRIs were decimated to 5120 triangles and used as the volume conductor. MNEs were computed from combined anatomical MRI and EEG data.⁵⁹⁻⁶¹ For inverse computations, the cortical surface from FreeSurfer was decimated to 4098 vertices per hemisphere; the source space was restricted to cortical gray matter; and orientations were restricted to be perpendicular to the local curvature of the cortical surface.⁶² The noise covariance matrix was obtained from the

prestimulus interval (−205 to −5 milliseconds) of the Before condition of each visit. The evoked response time courses were then computed for each vertex, separately for the Before, After[1], and After[2] conditions.^{34,63}

Because the ccPAS-modulated synapses were in the right M1, the time courses were extracted from a region of interest (ROI) in the right M1 area identified with the TMS-induced E-field estimates thresholded at 80% of the individual maximum (Fig. 2). In the control experiment for directionality, the time courses were instead extracted from the left M1 during right M1 stimulation. The additional control region in the right prefrontal cortex was picked from the FreeSurfer cortical parcellation. These ROIs contained several vertex points, each with its own time course. Each time course was baseline corrected from −200 to −10 milliseconds, averaged across vertex points within the ROI, and rectified (absolute value). Finally, the resulting ROI time courses were visually inspected, and any conditions in which the TMS pulse artifact persisted at latencies > 5 milliseconds or the prestimulus baseline noise levels differed between Before/After[1]/After[2] were removed from further analysis. Owing to these strict quality requirements, although there were 11 patients who produced ccPAS data in which at least one condition passed these criteria, for the numerical analyses, the final N was smaller for each condition (for the 14-millisecond asynchrony $N=7$ for both After[1] and After[2]); for the 9-millisecond asynchrony $N=6$ for After[1], $N=7$ for After[2]; for the 4-millisecond asynchrony $N=8$ for After[1], $N=7$ for After[2].

Statistical Analysis: Linear Mixed Model and Post Hoc Tests

To quantify the response amplitudes, the MNE time courses were averaged across 5 to 20 milliseconds (area under the curve, AUC); the statistical analyses below used their $\log(10)$ values. First, in an auxiliary analysis that was separate from the main analysis, to exclude the possibility that there were session-specific excitability differences unrelated to ccPAS, we compared the Before AUC amplitudes (dependent variable) across the three Asynchrony conditions (14/9/4 milliseconds, independent variables) using a linear mixed model (LMM). Then, in our main analysis for the ccPAS effects, the After[1] and After[2] responses were first normalized within sessions relative to the Before values. Note that latencies > 20 milliseconds were excluded because they have been suggested to be contaminated by artifacts from TMS tactile and acoustic stimulation⁶⁴ and/or confounded by recurrent activations back-projecting from other areas and indirect connections;⁶⁵ latencies < 20 milliseconds do not suffer from these issues because of delays in sensory and interregional pathways, even if they are more prone to extracranial TMS artifacts. Some subjects were not available for all three ccPAS asynchrony conditions, and some sessions were rejected owing to data quality, causing missing values incompatible with an analysis of variance. Therefore, we used the LMM method implemented in SPSS (version 27, IBM, Chicago, IL) that compensates for the effects of missing values using maximum likelihood techniques.^{66,67} Specifically, the AUC values from After[1] and After[2] were entered into an LMM with asynchrony as a continuous covariate (14/9/4 milliseconds zero-meaned to +5/0/−5 milliseconds, respectively), time (After[1]/After[2]) as a factor, and AUC response amplitude as the dependent variable. Fixed effects (asynchrony, time, and interaction asynchrony * time) were analyzed using a maximum likelihood estimator and a diagonal design matrix. Finally, for post hoc tests, the normalized response amplitudes were analyzed

with the nonparametric Kruskal-Wallis test. Significance threshold was $p = 0.05$ (two-tailed). Post hoc tests were only computed for areas in which the LMM result for asynchrony was significant.

Bayesian Post Hoc Statistics

We also used Bayesian inference to analyze the same AUC values as above because Bayesian statistics are considered to be robust even with relatively few observations.⁶⁸ Specifically, we used Bayesian t -tests implemented in SPSS (version 27), with Diffuse prior and Rouder's method.⁶⁹ We report the posterior significance (p), Bayes Factor (BF) values, and 95% credible intervals (CI). Significance threshold was $p = 0.05$ (two-tailed). Again, post hoc tests were only computed for areas in which the LMM result for asynchrony was significant.

RESULTS

Diffusion MRI Tractography

Figure 3 shows the group-level tractography results, consistent with a strong transcallosal axonal connection between the stimulated areas in the left and right M1 (similar results^{26,28}).

TMS-EEG Results From the Main Experiment

Figure 4 (left) shows group-level ccEP time courses extracted from the right M1, evoked by spTMS to the left M1, separately for the three different asynchronies (14, 9, 4 milliseconds) and time points (Before, After[1], After[2]). As expected, the nonphysiological TMS pulse artifact at approximately 0 milliseconds was much larger than the physiological range of EEG signals. However, the initial TMS artifact decayed quickly, in 5 milliseconds. Note that within each asynchrony visit, the TMS pulse artifact should be similar across the three time points (Before, After[1], After[2]) because the neuronavigated TMS coil location, all TMS parameters, and the EEG electrodes, leads, and impedances were kept constant within each visit. Based on the previously carefully characterized interhemispheric transcallosal conduction delays of 5 to 10 milliseconds between the motor cortices in previous literature,^{29,30} we expected that the ccEPs and therefore ccPAS effects would also be maximal around the conduction delay, which was supported by these results, in which particularly the 14- and 9-millisecond conditions showed clear deflections in this time window (note that the TMS pulse is very brief, only approximately 0.2 milliseconds, and therefore we are no longer injecting energy into the system at the time when the responses begin to rise at approximately 5 milliseconds). The responses also extended to somewhat longer latencies, consistent with the transcallosal bundle comprising axons with different conduction velocities.^{30,70–72} For statistics, we first confirmed in the auxiliary analysis using LMM that there were no clear differences between the Before conditions of the three Asynchrony conditions ($df = 13.39$, $F = 0.02$, significance = 0.88). Next, our main analysis of the ccPAS effects using an LMM found a significant effect for Asynchrony ($df = 24.70$, $F = 14.9$, significance = 0.001) but not for time ($df = 33.31$, $F = 0.01$, significance = 0.91). The interaction asynchrony * time was nonsignificant ($df = 25.19$, $F = 0.07$, significance = 0.80).

Figure 4 (right) depicts the corresponding AUC amplitudes (mean \pm SEM, After[1]/After[2] normalized relative to the Before condition).

Kruskal-Wallis post hoc tests comparing the After AUC values across the three asynchrony conditions found significant differences between 4- and 14-millisecond asynchronies at both After[1] ($p = 0.028$) and After[2] ($p = 0.013$). Other comparisons were not significant (After [1] 4 milliseconds vs 9 milliseconds $p = 0.519$ and 9 milliseconds vs 14 milliseconds $p = 0.317$; After[2] 4 milliseconds vs 9 milliseconds $p = 0.949$ and 9 milliseconds vs 14 milliseconds borderline significant at $p = 0.064$). In comparisons between the Before vs After time points, the asynchrony of 14 milliseconds increased the response amplitude significantly at After[1] ($p = 0.012$) and a nonsignificant trend at After[2] ($p = 0.132$), whereas 4 milliseconds decreased response amplitudes significantly at After [2] ($p = 0.012$) but not at After[1] ($p = 0.369$). As predicted, 9 milliseconds showed no significant changes or even trends at either time point (After[1] $p = 1.00$; After[2] $p = 0.633$). These results were consistent with STDP mechanisms. Supplementary Data Figure S2 illustrates the corresponding whisker plots.

Bayesian comparisons of the After AUC values across the three asynchrony conditions found a significant difference between 4- and 14-millisecond asynchronies at both After[1] ($p = 0.032$ BF = 0.425 CI = -0.004 to 0.541) and After[2] ($p = 0.009$ BF = 0.160 CI = 0.052 to 0.430). There was also a difference at After[2] between the 9- and 14-millisecond asynchronies ($p = 0.050$ BF = 0.573 CI = -0.033 to 0.578). Other comparisons were nonsignificant (After [1] 4 milliseconds vs 9 milliseconds $p = 0.547$ BF = 2.423 CI = -0.262 to 0.422 and 9 milliseconds vs 14 milliseconds $p = 0.214$ BF = 1.462 CI = -0.179 to 0.556; After[2] 4 milliseconds vs 9 milliseconds $p = 0.792$ BF = 2.752 CI = -0.317 to 0.254). In Bayesian comparisons between the Before and After time points, the asynchrony of 14 milliseconds showed at After[1] a nonsignificant trend toward increasing the response amplitude from Before values ($p = 0.097$ BF = 0.925 CI = -0.069 to 0.361); at After[2], this difference was significant ($p = 0.047$ BF = 0.561 CI = -0.026 to 0.283). For 4-millisecond asynchrony, there was a decreasing amplitude pattern from Before to After (After[1] $p = 0.107$ BF = 1.007 CI = -0.290 to 0.046; After[2] $p = 0.018$ BF = 0.276 CI = -0.221 to 0.003). As predicted, for asynchrony of 9 milliseconds, there were no significant changes or trends (After[1] $p = 0.698$ BF = 2.587 CI = -0.339 to 0.255; After[2] $p = 0.207$ BF = 1.469 CI = -0.407 to 0.120). Therefore, the Bayesian results followed the conventional statistical results.

TMS–EEG Results for the Control Experiments

Figure 5 shows results from the control experiment for directionality from the left hemisphere (spTMS to the right hemisphere). All three asynchrony conditions showed some deflections in the expected time window. For the 5- to 20-millisecond AUC response amplitudes, none of the effects were significant (asynchrony $df = 25.83$, $F = 1.15$, significance = 0.29; time $df = 37.64$, $F = 0.27$, significance = 0.61; interaction asynchrony * time $df = 25.3$, $F = 0.34$, significance = 0.56). Therefore, in the left M1, as predicted, there were no differences between asynchronies, which is inconsistent with STDP mechanisms

and consistent with the hypotheses for left M1. Supplementary Data Figure S3 shows the corresponding whisker plots.

Supplementary Data Figure S4 shows the AUC results from the control experiment for spatial specificity (right pars triangularis). Similarly to the control experiment for directionality, the amplitudes appeared to increase briefly at After[1], regardless of asynchrony, and then decreased at After[2]. For the LMM analysis, none of the effects was significant (asynchrony $df = 25.49$, $F = 0.01$, significance = 0.92; time $df = 33.92$, $F = 3.16$, significance = 0.08; asynchrony * time $df = 26.52$, $F = 1.21$, significance = 0.28). Supplementary Data Figure S5 shows the MEPs, suggesting that rMT was exceeded during spTMS.

DISCUSSION

ccPAS mechanisms in humans have thus far mainly been inferred from paired associative stimulation (PAS) studies that couple TMS of M1 with peripheral nerve stimulation (PNS).^{73–75} PAS likely relies on STDP because the asynchrony between TMS and PNS, adjusted by conduction delays, determines whether the MEPs are increased or decreased.^{33,73,75} Furthermore, blocking NMDA receptors prevents such MEP changes.⁷⁴ However, a recent PAS study in rodents that parametrically varied the stimulation parameters failed to observe any effects.⁷⁶ PAS effects in humans have varied strongly between subjects,^{77–79} and some placebo-controlled PAS studies in patients with stroke found no difference between PAS and sham.^{80,81} Moreover, a recent study suggested that low-frequency spTMS alone, when given at a strong intensity (such as during the test phase of PAS/ccPAS protocols), could be responsible for previously reported effects.⁸² The results in this study suggest that ccPAS effects in humans are likely mediated by STDP. This facilitates choosing optimal asynchronies in future research and clinical ccPAS protocols.

Previous ccPAS-EEG studies have introduced the use of EEG to assess ccPAS effects.^{83–85} However, they have relied on sensor-level TMS-evoked potential (TEP) analyses that cannot accurately localize the cortical modulation sites;⁸⁶ these studies were also limited to latencies ~ 11 milliseconds owing to TMS–EEG artifacts. The presently reported source-space ccEPs peaking at 5 to 10 milliseconds (Figs. 4 and 5) overlap with the early latency windows that most previous studies have avoided because of the TMS–EEG artifacts that are strongest during each ~ 0.2 -millisecond TMS pulse and thereafter decay over several milliseconds. To increase the possibility of observing neuronal activity at such early latencies, we reduced the duration of TMS artifacts by carefully optimizing recording techniques, including orienting each EEG lead for minimal induction from the TMS coil (Materials and Methods for details). Furthermore, we reduced the spatial spread of the artifact by choosing the ccPAS target/readout area in the hemisphere contralateral from where spTMS was delivered in an area with relatively little scalp muscle. We also used EEG source analysis, which acts as a spatial filter that suppresses artifacts more effectively than do sensor-level TEP signals that have a wider point-spread function.^{86,87} At the same time, we cannot exclude the possibility that some TMS pulse artifact may have leaked into our time window of interest, generating a superposition of an artifact and neuronally driven responses. However, the artifact should be relatively constant, which

is useful. On the basis of the results, it appears that the signals picked up a sufficient amount of neuronal activity because the modulations followed STDP, which is a neuronal property. Finally, the responses, showing evoked-response-type deflections in five of six conditions (Figs. 4 and 5), appeared in the exact time window where they should be, based on results from bifocal TMS interhemispheric inhibition^{29,30} and tractography⁸⁸ studies suggesting that the M1–M1 transcallosal conduction delay in the human brain is 5 to 10 milliseconds. Therefore, multiple results lined up in a way that supports a neuronal original of the ccEPs; conversely, if the ccEP differences were contaminated by artifacts, it would be highly unlikely to observe a set of results that aligns this well with the a priori hypotheses. These results open the possibility of capturing early latencies to quantify connectivity at physiologically relevant timescales. The findings also illustrate the potential of using EEG source localization techniques to probe population-level synaptic modulations at the desired cortical locations.

The control experiment for directionality showed that, as predicted, effects consistent with STDP mechanisms were not observed in left M1. Somewhat surprisingly, the amplitudes appeared to increase in the left M1 after ccPAS. This was unexpected because both the spTMS and ccPAS protocols delivered the TMS pulses at 5-second intervals, which should be too slow to result in persistent (non-STDP) changes in neuronal excitability.³² However, these changes were similar regardless of asynchrony, possibly reflecting non-STDP effects from spTMS delivered during the ccEP recordings that has recently been suggested to result in short-term modulations.⁸² Therefore, in terms of STDP, the effects were unidirectional (for $A \rightarrow B$ but not for $B \rightarrow A$). Previous ccPAS–EEG studies^{83–85} have instead reversed the direction of ccPAS modulation (separately for $A \rightarrow B$ and $B \rightarrow A$ with positive asynchronies only), which tests a different phenomenon.

Unifocal (one-coil) repetitive TMS (rTMS) and theta burst stimulation (TBS) have been widely used for research and clinical purposes. They result in network-level excitability and functional connectivity changes that include the directly stimulated “primary” area and any connectivity-based “secondary” regions throughout the brain.⁸⁹ However, functional MRI studies have suggested that connectivity may be decreased for some connections and increased for others, and the changes seem to spread beyond the intended network.⁹⁰ Moreover, frequency dependence of rTMS/TBS effects on primary areas (increased vs decreased excitability) and interregional connectivity may vary across brain regions.^{91–93} Thus, adjusting network connectivity with unifocal TMS is difficult because there is little control over where the connectivity changes occur and whether any specific connection is up- or downregulated. ccPAS is more selective than such unifocal TMS protocols because connectivity is adjusted between the two stimulated regions, and the asynchrony should allow increasing vs decreasing connectivity. Furthermore, ccPAS modulates effective (unidirectional) connectivity, whereas the directionality of unifocal TMS protocols is not clear because it is typically examined with measures that reflect functional (bidirectional) connectivity. On the basis of the present results and previous literature, it also appears that PAS/ccPAS effects may be more long-lasting than those of unifocal protocols,^{73–75,83,84,94} which would be useful for therapeutic purposes.

Limitations of the study include a relatively small number of subjects, which was mainly driven by the strict data quality criteria required to capture early response components. To observe short-latency components, we used stricter criteria in this study than in many previous studies. To attempt to balance out the relatively small number of subjects, we included several experimental conditions and control experiments that, together with the strong statistical results, allow making conclusions that a larger sample size with a simpler design could not. In addition, we delivered spTMS at an intensity of 100% rMT, which may have not been sufficient to induce strong transcallosal responses in some participants and/or conditions; it is of note, however, that increasing the intensity also strengthens the spTMS-evoked artifacts.^{47,48} We also analyzed the data with both conventional nonparametric statistics and Bayesian tests that are less sensitive to sample size limitations,⁶⁸ and the results were very similar. More TMS–EEG technologic innovations and studies are needed to increase the reliability of observing short-latency ccEPs.

CONCLUSIONS

ccPAS selectively up- or downregulated effective connectivity between the stimulated areas. The effects were consistent with STDP mechanisms because they were temporally selective (ie, depending on the order of pre- vs postsynaptic activations, which was parametrically varied with the asynchrony values), were unidirectional, and seemed to be spatially selective to the modulated connection. The data also suggest that short-latency ccEPs starting as early as 5 milliseconds might be useful to detect ccPAS effects. These findings clarify the mechanisms of ccPAS in humans, pave the way to determining optimal asynchronies in such experiments, and open new venues for targeted modulation of cortico-cortical connectivity for research and clinical applications.

Supplementary Material

Refer to Web version on PubMed Central for supplementary material.

Acknowledgements

The authors thank Matti Hämäläinen, Jyrki Ahveninen, Aapo Nummenmaa, Jennifer McNab, Anastasia Yendiki, Thomas Witzel, Todd Parrish, Yevgenia Kozorovitskiy, Daria Porter, Sudarshan Srivitsan, and Molly Hermiller for assistance and advice.

Source(s) of financial support:

The study was funded by Dr. Ralph and Marian Falk Medical Research Trust Catalyst Grant (Tommi Raij), Northwestern University Core support (Tommi Raij), and National Institutes of Health (NIH) R01NS095251 (Lee E. Miller), with support from the NIH Shared Instrumentation Grant 1S10OD020080-01.

REFERENCES

1. Katz LC, Shatz CJ. Synaptic activity and the construction of cortical circuits. *Science*. 1996;274:1133–1138. [PubMed: 8895456]
2. Xia CH, Ma Z, Ciric R, et al. Linked dimensions of psychopathology and connectivity in functional brain networks. *Nat Commun*. 2018;9:3003. [PubMed: 30068943]
3. Forkel SJ, Catani M. Lesion mapping in acute stroke aphasia and its implications for recovery. *Neuropsychologia*. 2018;115:88–100. [PubMed: 29605593]

4. Filley CM, Fields RD. White matter and cognition: making the connection. *J Neurophysiol.* 2016;116:2093–2104. [PubMed: 27512019]
5. Schmahmann JD, Smith EE, Eichler FS, Filley CM. Cerebral white matter: neuroanatomy, clinical neurology, and neurobehavioral correlates. *Ann N Y Acad Sci.* 2008;1142:266–309. [PubMed: 18990132]
6. Sozmen EG, Hinman JD, Carmichael ST. Models that matter: white matter stroke models. *Neurotherapeutics.* 2012;9:349–358. [PubMed: 22362423]
7. Corbetta M, Ramsey L, Callejas A, et al. Common behavioral clusters and subcortical anatomy in stroke. *Neuron.* 2015;85:927–941. [PubMed: 25741721]
8. Jackson A, Mavoori J, Fetz EE. Long-term motor cortex plasticity induced by an electronic neural implant. *Nature.* 2006;444:56–60. [PubMed: 17057705]
9. Seeman SC, Mogen BJ, Fetz EE, Perlmutter SI. Paired stimulation for spike-timing-dependent plasticity in primate sensorimotor cortex. *J Neurosci.* 2017;37:1935–1949. [PubMed: 28093479]
10. Rebesco JM, Stevenson IH, Kording KP, Solla SA, Miller LE. Rewiring neural interactions by micro-stimulation. *Front Syst Neurosci.* 2010;4:39. [PubMed: 20838477]
11. Bi GQ, Poo MM. Synaptic modifications in cultured hippocampal neurons: dependence on spike timing, synaptic strength, and postsynaptic cell type. *J Neurosci.* 1998;18:10464–10472. [PubMed: 9852584]
12. Magee JC, Johnston D. A synaptically controlled, associative signal for Hebbian plasticity in hippocampal neurons. *Science.* 1997;275:209–213. [PubMed: 8985013]
13. Markram H, Lübke J, Frotscher M, Sakmann B. Regulation of synaptic efficacy by coincidence of postsynaptic APs and EPSPs. *Science.* 1997;275:213–215. [PubMed: 8985014]
14. Jacob V, Brasier DJ, Erchova I, Feldman D, Shulz DE. Spike timing-dependent synaptic depression in the in vivo barrel cortex of the rat. *J Neurosci.* 2007;27:1271–1284. [PubMed: 17287502]
15. Rebesco JM, Miller LE. Enhanced detection threshold for in vivo cortical stimulation produced by Hebbian conditioning. *J Neural Eng.* 2011;8:016011. [PubMed: 21252415]
16. Rizzo V, Siebner HS, Morgante F, Mastroeni C, Girlanda P, Quartarone A. Paired associative stimulation of left and right human motor cortex shapes interhemispheric motor inhibition based on a Hebbian mechanism. *Cereb Cortex.* 2009;19:907–915. [PubMed: 18791179]
17. Koganemaru S, Mima T, Nakatsuka M, Ueki Y, Fukuyama H, Domen K. Human motor associative plasticity induced by paired bihemispheric stimulation. *J Physiol.* 2009;587:4629–4644. [PubMed: 19687124]
18. Koch G, Ponzo V, Di Lorenzo F, Caltagirone C, Veniero D. Hebbian and anti-Hebbian spike-timing-dependent plasticity of human cortico-cortical connections. *J Neurosci.* 2013;33:9725–9733. [PubMed: 23739969]
19. Kohl S, Hannah R, Rocchi L, Nord CL, Rothwell J, Voon V. Cortical paired associative stimulation influences response inhibition: cortico-cortical and cortico-subcortical networks. *Biol Psychiatry.* 2019;85:355–363. [PubMed: 29724490]
20. Nord CL, Popa T, Smith E, et al. The effect of frontoparietal paired associative stimulation on decision-making and working memory. *Cortex.* 2019;117:266–276. [PubMed: 31009813]
21. Ribolsi M, Lisi G, Ponzo V, et al. Left hemispheric breakdown of LTP-like cortico-cortical plasticity in schizophrenic patients. *Clin Neurophysiol.* 2017;128:2037–2042. [PubMed: 28843131]
22. Di Lorenzo F, Ponzo V, Motta C, et al. Impaired spike timing dependent cortico-cortical plasticity in Alzheimer’s disease patients. *J Alzheimers Dis.* 2018;66:983–991. [PubMed: 30372679]
23. Koch G. Cortico-cortical connectivity: the road from basic neurophysiological interactions to therapeutic applications. *Exp Brain Res.* 2020;238:1677–1684. [PubMed: 32705294]
24. Zibman S, Zangen A. Comments on “cortico-cortical connectivity: the road from basic neurophysiological interactions to therapeutic applications” (Koch, *Exp Brain Res.*, 2020). *Exp Brain Res.* 2021;239:2357–2358. [PubMed: 33751159]
25. Koch G. Response letter to comments on “cortico-cortical connectivity: the road from basic neurophysiological interactions to therapeutic applications” by Zibman and Zangen. *Exp Brain Res.* 2021;239:1685–1686. [PubMed: 33928398]

26. Ruddy KL, Leemans A, Carson RG. Transcallosal connectivity of the human cortical motor network. *Brain Struct Funct.* 2017;222:1243–1252. [PubMed: 27469272]
27. Voineskos AN, Farzan F, Barr MS, et al. The role of the corpus callosum in transcranial magnetic stimulation induced interhemispheric signal propagation. *Biol Psychiatry.* 2010;68:825–831. [PubMed: 20708172]
28. Wahl M, Lauterbach-Soon B, Hattingen E, et al. Human motor corpus callosum: topography, somatotopy, and link between microstructure and function. *J Neurosci.* 2007;27:12132–12138. [PubMed: 17989279]
29. Ferbert A, Priori A, Rothwell JC, Day BL, Colebatch JG, Marsden CD. Interhemispheric inhibition of the human motor cortex. *J Physiol.* 1992;453:525–546. [PubMed: 1464843]
30. Ni Z, Leodori G, Vial F, et al. Measuring latency distribution of transcallosal fibers using transcranial magnetic stimulation. *Brain Stimul.* 2020;13:1453–1460. [PubMed: 32791313]
31. Oldfield RC. The assessment and analysis of handedness: the Edinburgh Inventory. *Neuropsychologia.* 1971;9:97–113. [PubMed: 5146491]
32. Rossi S, Hallett M, Rossini PM, Pascual-Leone A. Safety of TMS Consensus Group. Safety, ethical considerations, and application guidelines for the use of transcranial magnetic stimulation in clinical practice and research. *Clin Neurophysiol.* 2009;120:2008–2039. [PubMed: 19833552]
33. Suppa A, Quartarone A, Siebner H, et al. The associative brain at work: evidence from paired associative stimulation studies in humans. *Clin Neurophysiol.* 2017;128:2140–2164. [PubMed: 28938144]
34. Gramfort A, Luessi M, Larson E, et al. MNE software for processing MEG and EEG data. *Neuroimage.* 2014;86:446–460. [PubMed: 24161808]
35. Hämäläinen M, Hari R, Ilmoniemi RJ, Knuutila J, Lounasmaa OV. Magnetoencephalography: theory, instrumentation, and application to noninvasive studies of the working human brain. *Rev Mod Phys.* 1993;65:413–497.
36. Murakami S, Okada Y. Contributions of principal neocortical neurons to magnetoencephalography and electroencephalography signals. *J Physiol.* 2006;575:925–936. [PubMed: 16613883]
37. Reis J, Swayne OB, Vandermeeren Y, et al. Contribution of transcranial magnetic stimulation to the understanding of cortical mechanisms involved in motor control. *J Physiol.* 2008;586:325–351. [PubMed: 17974592]
38. Rossini PM, Barker AT, Berardelli A, et al. Non-invasive electrical and magnetic stimulation of the brain, spinal cord and roots: basic principles and procedures for routine clinical application. Report of an IFCN committee. *Electroencephalogr Clin Neurophysiol.* 1994;91:79–92. [PubMed: 7519144]
39. van der Kouwe AJW, Benner T, Salat DH, Fischl B. Brain morphometry with multiecho MPRage. *NeuroImage.* 2008;40:559–569. [PubMed: 18242102]
40. Wedeen VJ, Hagmann P, Tseng WY, Reese TG, Weisskoff RM. Mapping complex tissue architecture with diffusion spectrum magnetic resonance imaging. *Magn Reson Med.* 2005;54:1377–1386. [PubMed: 16247738]
41. Setsompop K, Cohen-Adad J, Gagoski BA, et al. Improving diffusion MRI using simultaneous multi-slice echo planar imaging. *Neuroimage.* 2012;63:569–580. [PubMed: 22732564]
42. Fischl B. FreeSurfer. *Neuroimage.* 2012;62:774–781. [PubMed: 22248573]
43. Behrens TE, Woolrich MW, Jenkinson M, et al. Characterization and propagation of uncertainty in diffusion-weighted MR imaging. *Magn Reson Med.* 2003;50:1077–1088. [PubMed: 14587019]
44. Postelnicu G, Zollei L, Fischl B. Combined volumetric and surface registration. *IEEE Trans Med Imaging.* 2009;28:508–522. [PubMed: 19273000]
45. Zöllei L, Stevens A, Huber K, Kakunoori S, Fischl B. Improved tractography alignment using combined volumetric and surface registration. *Neuroimage.* 2010;51:206–213. [PubMed: 20153833]
46. Ilmoniemi RJ, Hernandez-Pavon JC, Makela NN, et al. Dealing with artifacts in TMS-evoked EEG. *Annu Int Conf IEEE Eng Med Biol Soc.* 2015;2015:230–233. [PubMed: 26736242]
47. Mutanen T, Mäki H, Ilmoniemi RJ. The effect of stimulus parameters on TMS-EEG muscle artifacts. *Brain Stimul.* 2013;6:371–376. [PubMed: 22902312]

48. Ilmoniemi RJ, Kici D. Methodology for combined TMS and EEG. *Brain Topogr.* 2010;22:233–248. [PubMed: 20012350]
49. Hernandez-Pavon JC, Kugiumtzis D, Zrenner C, Kimiskidis VK, Metsomaa J. Removing artifacts from TMS-evoked EEG: a methods review and a unifying theoretical framework. *J Neurosci Methods.* 2022;376:109591. [PubMed: 35421514]
50. Terao Y, Ugawa Y. Basic mechanisms of TMS. *J Clin Neurophysiol.* 2002;19:322–343. [PubMed: 12436088]
51. Klem GH, Lüders HO, Jasper HH, Elger C. The ten-twenty electrode system of the international federation. *The International Federation of Clinical Neurophysiology. Electroencephalogr Clin Neurophysiol Suppl.* 1999;52:3–6. [PubMed: 10590970]
52. Sekiguchi H, Takeuchi S, Kadota H, Kohno Y, Nakajima Y. TMS-induced artifacts on EEG can be reduced by rearrangement of the electrode's lead wire before recording. *Clin Neurophysiol.* 2011;122:984–990. [PubMed: 20920887]
53. Nummenmaa A, Stenroos M, Ilmoniemi RJ, Okada YC, Hämäläinen MS, Raij T. Comparison of spherical and realistically shaped boundary element head models for transcranial magnetic stimulation navigation. *Clin Neurophysiol.* 2013;124:1995–2007. [PubMed: 23890512]
54. Stenroos M, Mäntynen V, Nenonen J. A MATLAB library for solving quasi-static volume conduction problems using the boundary element method. *Comput Methods Programs Biomed.* 2007;88:256–263. [PubMed: 18022274]
55. Rogasch NC, Sullivan C, Thomson RH, et al. Analysing concurrent transcranial magnetic stimulation and electroencephalographic data: a review and introduction to the open-source TESA software. *NeuroImage.* 2017;147:934–951. [PubMed: 27771347]
56. Hernandez-Pavon JC, Metsomaa J, Mutanen T, et al. Uncovering neural independent components from highly artifactual TMS-evoked EEG data. *J Neurosci Methods.* 2012;209:144–157. [PubMed: 22687937]
57. Korhonen RJ, Hernandez-Pavon JC, Metsomaa J, Mäki H, Ilmoniemi RJ, Sarvas J. Removal of large muscle artifacts from transcranial magnetic stimulation-evoked EEG by independent component analysis. *Med Biol Eng Comput.* 2011;49:397–407. [PubMed: 21331656]
58. Bertazzoli G, Esposito R, Mutanen TP, et al. The impact of artifact removal approaches on TMS–EEG signal. *Neuroimage.* 2021;239:118272. [PubMed: 34144161]
59. Dale AM, Sereno MI. Improved localization of cortical activity by combining EEG and MEG with MRI cortical surface reconstruction: a linear approach. *J Cogn Neurosci.* 1993;5:162–176. [PubMed: 23972151]
60. Dale AM, Liu AK, Fischl BR, et al. Dynamic statistical parametric mapping: combining fMRI and MEG for high-resolution imaging of cortical activity. *Neuron.* 2000;26:55–67. [PubMed: 10798392]
61. Liu AK, Belliveau JW, Dale AM. Spatiotemporal imaging of human brain activity using functional MRI constrained magnetoencephalography data: Monte Carlo simulations. *Proc Natl Acad Sci USA.* 1998;95:8945–8950. [PubMed: 9671784]
62. Lin FH, Belliveau JW, Dale AM, Hämäläinen MS. Distributed current estimates using cortical orientation constraints. *Hum Brain Mapp.* 2006;27:1–13. [PubMed: 16082624]
63. Hämäläinen MS, Ilmoniemi RJ. Interpreting magnetic fields of the brain: minimum norm estimates. *Med Biol Eng Comput.* 1994;32:35–42. [PubMed: 8182960]
64. Conde V, Tomasevic L, Akopian I, et al. The non-transcranial TMS-evoked potential is an inherent source of ambiguity in TMS-EEG studies. *Neuroimage.* 2019;185:300–312. [PubMed: 30347282]
65. Chiappini E, Borgomaneri S, Marangon M, Turrini S, Romei V, Avenanti A. Driving associative plasticity in premotor-motor connections through a novel paired associative stimulation based on long-latency cortico-cortical interactions. *Brain Stimul.* 2020;13:1461–1463. [PubMed: 32791314]
66. Ibrahim JG, Molenberghs G. Missing data methods in longitudinal studies: a review. *Test (Madr).* 2009;18:1–43. [PubMed: 21218187]
67. McCulloch C, Searle S, Neuhaus J. *Generalized, Linear, and Mixed Models.* 2nd ed. Wiley; 2008.
68. Kording KP. Bayesian statistics: relevant for the brain? *Curr Opin Neurobiol.* 2014;25:130–133. [PubMed: 24463330]

69. Rouder JN, Speckman PL, Sun D, Morey RD, Iverson G. Bayesian t tests for accepting and rejecting the null hypothesis. *Psychon Bull Rev.* 2009;16:225–237. [PubMed: 19293088]
70. Caminiti R, Carducci F, Piervincenzi C, et al. Diameter, length, speed, and conduction delay of callosal axons in macaque monkeys and humans: comparing data from histology and magnetic resonance imaging diffusion tractography. *J Neurosci.* 2013;33:14501–14511. [PubMed: 24005301]
71. Nunez PL, Srinivasan R. Neocortical dynamics due to axon propagation delays in cortico-cortical fibers: EEG traveling and standing waves with implications for topdown influences on local networks and white matter disease. *Brain Res.* 2014;1542:138–166. [PubMed: 24505628]
72. Nunez PL, Srinivasan R, Fields RD. EEG functional connectivity, axon delays and white matter disease. *Clin Neurophysiol.* 2015;126:110–120. [PubMed: 24815984]
73. Stefan K, Kunesch E, Cohen LG, Benecke R, Classen J. Induction of plasticity in the human motor cortex by paired associative stimulation. *Brain.* 2000;123:572–584. [PubMed: 10686179]
74. Stefan K, Kunesch E, Benecke R, Cohen LG, Classen J. Mechanisms of enhancement of human motor cortex excitability induced by interventional paired associative stimulation. *J Physiol.* 2002;543:699–708. [PubMed: 12205201]
75. Wolters A, Sandbrink F, Schlottmann A, et al. A temporally asymmetric Hebbian rule governing plasticity in the human motor cortex. *J Neurophysiol.* 2003;89:2339–2345. [PubMed: 12612033]
76. Ting WK, Huot-Lavoie M, Ethier C. Paired associative stimulation fails to induce plasticity in freely behaving intact rats. *eNeuro.* 2020;7:ENEURO.0396–19.2020.
77. Müller-Dahlhaus JF, Orekhov Y, Liu Y, Ziemann U. Interindividual variability and age-dependency of motor cortical plasticity induced by paired associative stimulation. *Exp Brain Res.* 2008;187:467–475. [PubMed: 18320180]
78. Minkova L, Peter J, Abdulkadir A, et al. Determinants of inter-individual variability in corticomotor excitability induced by paired associative stimulation. *Front Neurosci.* 2019;13:841. [PubMed: 31474818]
79. Campana M, Papazova I, Pross B, Hasan A, Strube W. Motor-cortex excitability and response variability following paired-associative stimulation: a proof-of-concept study comparing individualized and fixed inter-stimulus intervals. *Exp Brain Res.* 2019;237:1727–1734. [PubMed: 31025050]
80. Tarri M, Brihmat N, Gasq D, et al. Five-day course of paired associative stimulation fails to improve motor function in stroke patients. *Ann Phys Rehabil Med.* 2018;61:78–84. [PubMed: 29274471]
81. Palmer JA, Wolf SL, Borich MR. Paired associative stimulation modulates corticomotor excitability in chronic stroke: a preliminary investigation. *Restor Neurol Neurosci.* 2018;36:183–194. [PubMed: 29526858]
82. D’Amico JM, Dongés SC, Taylor JL. High-intensity, low-frequency repetitive transcranial magnetic stimulation enhances excitability of the human corticospinal pathway. *J Neurophysiol.* 2020;123:1969–1978. [PubMed: 32292098]
83. Veniero D, Ponzio V, Koch G. Paired associative stimulation enforces the communication between interconnected areas. *J Neurosci.* 2013;33:13773–13783. [PubMed: 23966698]
84. Casula EP, Pellicciari MC, Picazio S, Caltagirone C, Koch G. Spike-timing-dependent plasticity in the human dorso-lateral prefrontal cortex. *Neuroimage.* 2016;143:204–213. [PubMed: 27591116]
85. Zibman S, Daniel E, Alyagon U, Etkin A, Zangen A. Interhemispheric cortico-cortical paired associative stimulation of the prefrontal cortex jointly modulates frontal asymmetry and emotional reactivity. *Brain Stimul.* 2019;12:139–147. [PubMed: 30392898]
86. Schoffelen JM, Gross J. Source connectivity analysis with MEG and EEG. *Hum Brain Mapp.* 2009;30:1857–1865. [PubMed: 19235884]
87. Ilmoniemi RJ, Virtanen J, Ruohonen J, et al. Neuronal responses to magnetic stimulation reveal cortical reactivity and connectivity. *NeuroReport.* 1997;8:3537–3540. [PubMed: 9427322]
88. Berman S, Filo S, Mezer AA. Modeling conduction delays in the corpus callosum using MRI-measured g-ratio. *Neuroimage.* 2019;195:128–139. [PubMed: 30910729]

89. Fox MD, Halko MA, Eldaief MC, Pascual-Leone A. Measuring and manipulating brain connectivity with resting state functional connectivity magnetic resonance imaging (fcMRI) and transcranial magnetic stimulation (TMS). *Neuroimage*. 2012;62:2232–2243. [PubMed: 22465297]
90. Beynel L, Powers JP, Appelbaum LG. Effects of repetitive transcranial magnetic stimulation on resting-state connectivity: a systematic review. *Neuroimage*. 2020;211:116596. [PubMed: 32014552]
91. Castrillon G, Sollmann N, Kurcyus K, Razi A, Krieg SM, Riedl V. The physiological effects of noninvasive brain stimulation fundamentally differ across the human cortex. *Sci Adv*. 2020;6:eay2739. [PubMed: 32064344]
92. Hermiller MS, VanHaerents S, Raij T, Voss JL. Frequency-specific noninvasive modulation of memory retrieval and its relationship with hippocampal network connectivity. *Hippocampus*. 2019;29:595–609. [PubMed: 30447076]
93. Salinas FS, Franklin C, Narayana S, Szabó CÁ, Fox PT. Repetitive transcranial magnetic stimulation educes frequency-specific causal relationships in the motor network. *Brain Stimul*. 2016;9:406–414. [PubMed: 26964725]
94. Johnen VM, Neubert FX, Buch ER, et al. Causal manipulation of functional connectivity in a specific neural pathway during behaviour and at rest. *Elife*. 2015;4: e04585. [PubMed: 25664941]

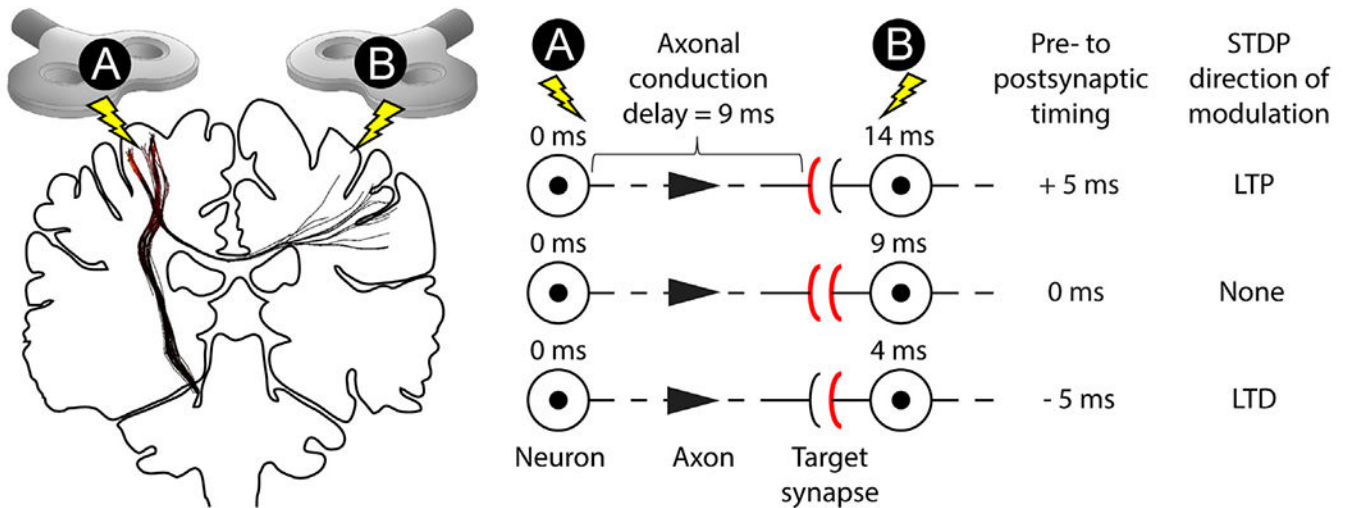


Figure 1.

Model of ccPAS and STDP. (Left) ccPAS can be delivered by stimulating two cortical areas, A and B, that are axonally connected (here, left and right M1, coronal slice with MRI tractography) with bifocal TMS. To induce STDP in area B, areas A and B are stimulated at slightly different times (“asynchrony”). Note that the axons are long-range, which results in an axonal conduction delay from area A to B (here, 9 milliseconds) that must be considered when selecting the asynchrony. (Right) During ccPAS, to induce STDP in the target synapse in area B, TMS pulses are delivered at three different asynchronies on separate days. The target synapse is shown with the presynaptic component (axon terminal) for a neuron originating in area A and the postsynaptic component (dendrite) for a neuron in area B; the black arrowheads indicate the direction of effective connectivity being considered in the main experiment analysis, and the red color indicates which side of the synapse is activated first. When the asynchrony is slightly longer than the conduction delay (top), presynaptic activations occur before postsynaptic, leading to strengthening of the target synapse, which results in increased effective connectivity $A \rightarrow B$. If the asynchrony equals the conduction delay (middle), both sides of the synapse are activated simultaneously, and there is no STDP. When the asynchrony is shorter than the conduction delay (bottom), synaptic efficacy at the target synapse decreases, which results in weaker effective connectivity $A \rightarrow B$. Note that the transcallosal connections between A and B are reciprocal; here, we only illustrate the direction from $A \rightarrow B$. Supplementary Data Figure S1 shows the pre- to postsynaptic timings in area A for the opposite $B \rightarrow A$ direction for the same ccPAS protocol (control experiment for directionality). LTD, long-term depression; LTP, long-term potentiation. [Color figure can be viewed at www.neuromodulationjournal.org]

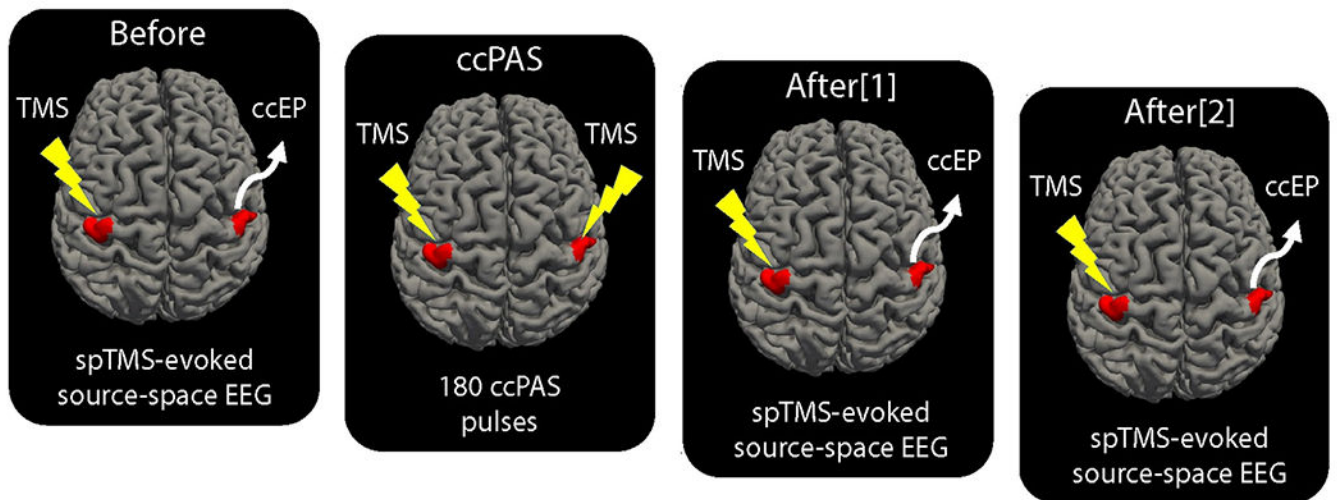


Figure 2.

Experimental design. To assess strengths of the target synapses before (Before) in addition to 10 minutes (After[1]) and 60 minutes (After [2]) after ccPAS, spTMS was delivered to the left M1 while extracting ccEPs from the right M1 (main experiment). In additional runs (not shown), spTMS was delivered to the right M1 while extracting ccEPs from the left M1 at the Before/After[1] / After[2] time points (control experiment for directionality). The ccPAS modulation consisted of delivering 180 TMS pulse pairs at a rate of 0.2 Hz, when the first pulse was delivered to the left M1 and the second pulse to the right M1, with asynchronies of 14 milliseconds, 9 milliseconds, or 4 milliseconds, on separate visits. Spatial extent of the TMS activations was estimated from the TMS-induced E-fields (red) that were also used for extracting the ccEPs from the right M1 (main experiment) and left M1 (control experiment for directionality). [Color figure can be viewed at www.neuromodulationjournal.org]

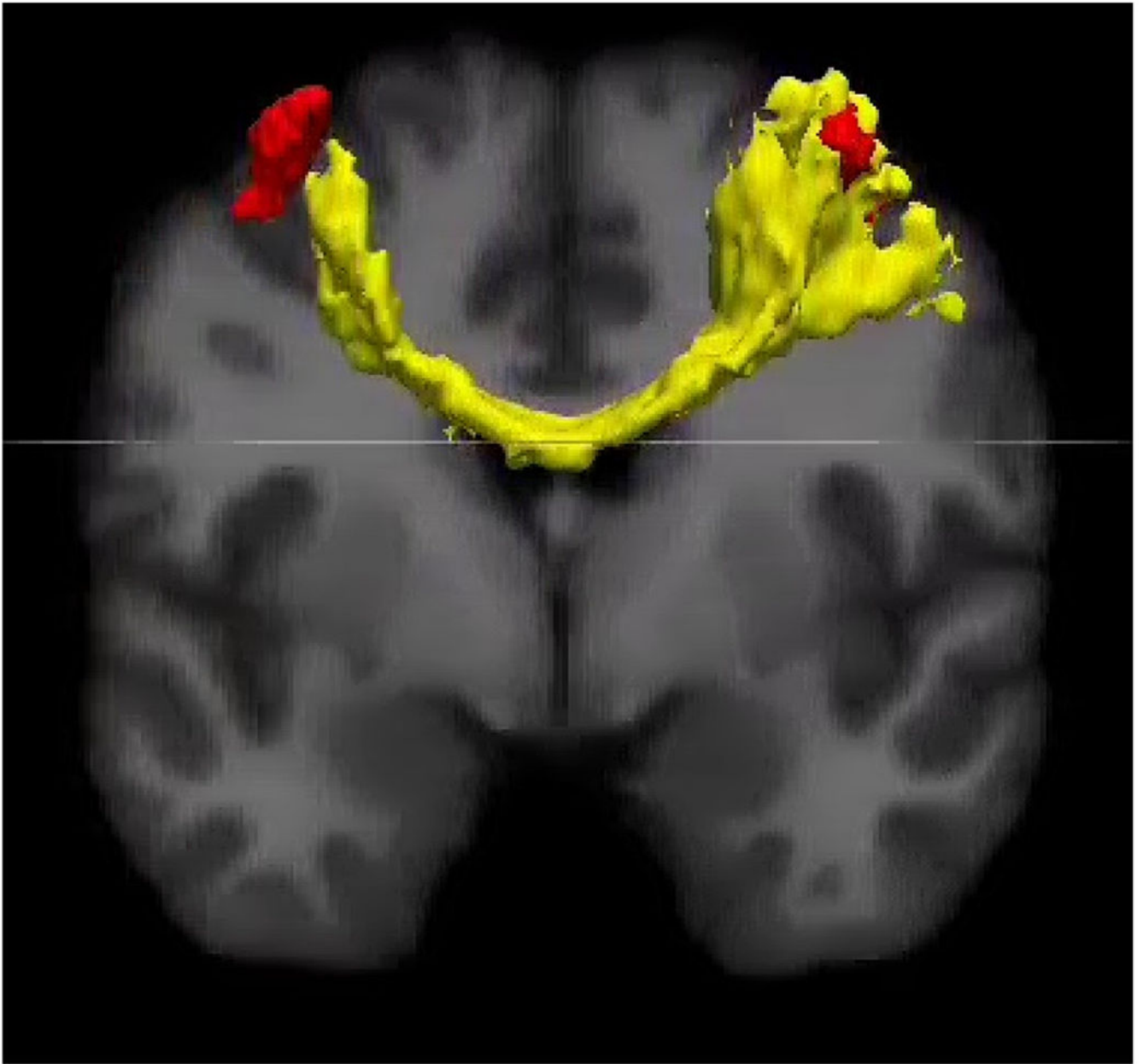


Figure 3. MRI tractography results. These group-level results ($N=7$) were recorded on a Siemens Prisma and a 64-channel receiver array using a simultaneous multislice sequence with 257 directions and a grid-sampling scheme with 22 different nonzero b values ranging between 150 and 4000. The left and right M1 (red), extracted from the TMS E-fields, were here used as seeds for probabilistic tractography (left M1 as seed, right M1 as waypoint mask). The tractography result (yellow) is consistent with a major transcallosal axonal bundle connecting the left and right M1. Coronal slice at the M1 level, posterior view (anatomical left on left). [Color figure can be viewed at www.neuromodulationjournal.org]

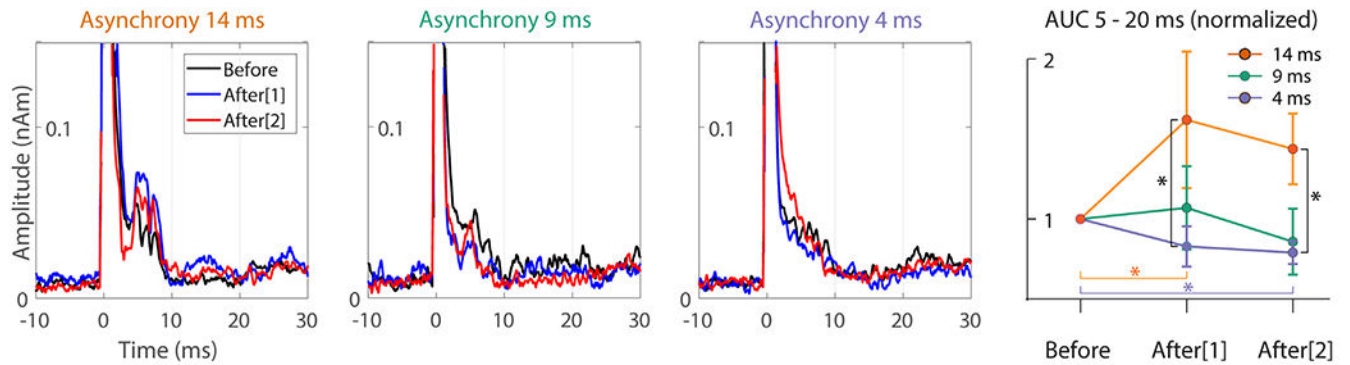


Figure 4.

Main experiment: ccEP time courses extracted from right M1. These group-level responses were recorded in the runs in which sPTMS was delivered to the left M1. (Left) The group-level nonnormalized time courses for the 14-millisecond, 9-millisecond, and 4-millisecond ccPAS asynchronies. After an initial TMS pulse artifact at approximately 0 to 4 milliseconds, there were well-defined evoked response components at approximately 5 to 10 milliseconds and longer-lasting deflections up to approximately 20 milliseconds, here most clearly seen in the 14-millisecond asynchrony data. Therefore, for statistical analysis, AUC values were extracted from the 5-to 20-millisecond time window for all conditions. (Right) The corresponding results for 5-to 20-millisecond AUC values (mean with SEM error bars). Consistent with STDP mechanisms, there were significant ($p < 0.05$) differences between the Asynchrony conditions (black vertical bars with stars) in addition to changes from Before PAS to the After[1]/After[2] PAS time points for the 14- and 4-millisecond asynchronies (colored horizontal bars with stars), and the changes occurred in the predicted directions. When comparing the time courses (three leftmost panels) with the AUC results (rightmost panel), note that the group-level time courses were averaged across subjects without normalization, whereas in the AUC analysis, the individual values were normalized relative to each subject's Before values. [Color figure can be viewed at www.neuromodulationjournal.org]

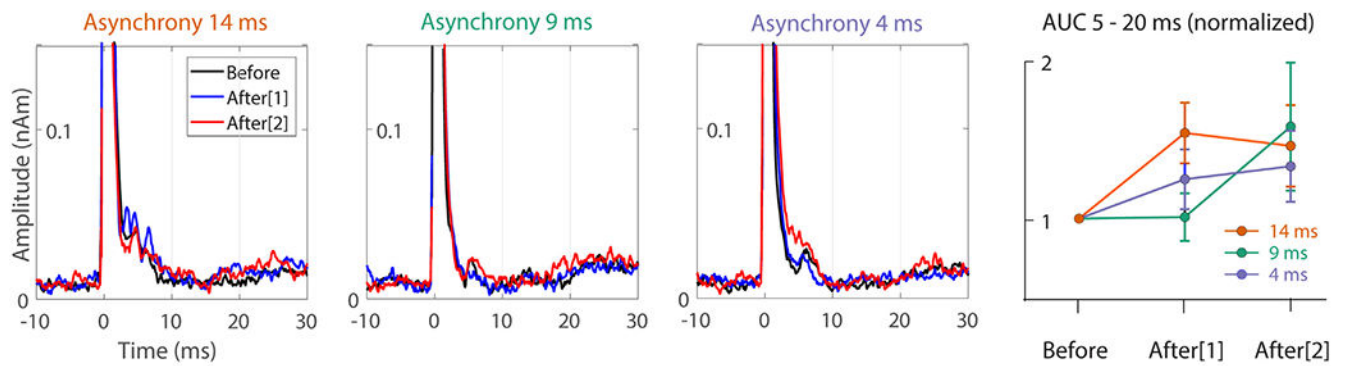


Figure 5.

Control experiment for directionality: ccEPs extracted from left M1. These group-level responses were recorded in the runs in which spTMS was delivered to the right M1. (Left) The nonnormalized group-level time courses between the 14-millisecond, 9-millisecond, and 4-millisecond ccPAS asynchronies. (Right) The corresponding AUC results for 5-to 20-millisecond amplitude values (mean with SEM error bars, normalized relative to the Before values). Although the response amplitudes increased from Before to After[1]/After[2], they did so regardless of Asynchrony, which is not consistent with STDP mechanisms, suggesting that, as predicted, the STDP effects were unidirectional. [Color figure can be viewed at www.neuromodulationjournal.org]